Anisotropic momentum distribution of positron-annihilation radiation in semiconductors

Mineo Saito
NEC Scientific Information System Development, Ltd., 34 Miyukigaoka, Tsukuba, Ibaraki 305, Japan

Atsushi Oshiyama
NEC Fundamental Research Laboratories, 34 Miyukigaoka, Tsukuba, Ibaraki 305, Japan

Shoichiro Tanigawa
Institute of Materials Science, University of Tsukuba, Tennoudai, Tsukuba, Ibaraki 305, Japan
(Received 1 July 1991)

Momentum distributions of positron-annihilation radiation with electrons in semiconductors are studied by use of first-principles calculations of the annihilation rates. For perfect crystals of Si and GaAs, the present calculation successfully reproduces the observed momentum distribution, in which a valley along the [100] line and a dip around the Γ point exist. An analysis based on group theory shows that both the valley and dip are consequences of the fact that the upper two valence bands make no contribution to the annihilation rates on the [100] line and at the Γ point. Furthermore, the case that a positron is captured by a neutral monovacancy in Si is studied by employing a supercell model in which the cell contains 53 Si atoms and one vacancy site. It is found that the valley and the dip in the momentum distribution observed in the perfect crystal disappear. It is proposed, from the drastic change in the momentum distribution upon vacancy introduction into the perfect crystal, that the angular correlation of annihilation radiation in the positron-annihilation technique is an effective tool for the detection of vacancies and for obtaining microscopic information about their electronic states. Finally, the lifetime of the captured positron is found to be sensitive to the small relaxation of the host atoms around the vacancy.

I. INTRODUCTION

The positron-annihilation technique has been established as a major tool for studying electron states and atomic defects in metals.[1] The recent development of the angular correlation of annihilation radiation (ACAR) technique enables us to obtain the three-dimensional momentum distribution of emitted photons. Since these photons are created by positron annihilation with electrons in a solid and the momentum distribution of the photons thus corresponds to that of the electrons, the method is considered to be an effective microscopic probe into the materials. An attractive target of this probe is any semiconductor in which the valence electrons are distributed mainly in the bond region and the distribution in space is thus prominently anisotropic. This anisotropy is reflected on the momentum distributions observed through ACAR in the positron-annihilation technique.

For elemental and compound semiconductors, interesting features of the electron-momentum distributions in the positron annihilation have been studied.[2–8] In an earlier stage, West, Mayers, and Walters[5] have performed experiments by conventional two-dimensional ACAR which gives integrated rates over an axis. It is shown, in their momentum distribution for Ge with the integration axis of $(1\bar{1}0)$, that a dip appears around the origin in the momentum space and that valleys appear along the [110] and [100] axes. Later, Tanigawa[6] found that, for the case of GaAs, these dips and valleys become shallow compared with the case of Ge. This interesting difference in momentum distributions between Ge and GaAs were studied by Chiba and Akahane,[7] calculating the positron-annihilation rates based on a parameter-adjusted linear combination of atomic orbitals method. They found that some valence bands do not contribute to the annihilation rate (annihilation inactive) when the photon momentum is parallel to the [100], [110], and [111] axes of Ge and that this situation is modified in the case of GaAs. They concluded that the difference in the annihilation inactive bands between Ge and GaAs is the origin of the different shape of the momentum distributions. It is thus expected that anisotropy also appears in the three-dimensional momentum distribution, in which the annihilation rate with the electron having the momentum p is not integrated along any axis.

Very recently, Tanigawa succeeded in measuring three-dimensional distribution.[8] The obtained momentum distributions of elemental and compound semiconductors on the (001) plane are found to be quite different from the previous ones obtained through the conventional two-dimensional ACAR. First, the momentum distribution shows a ridge along the [110] line and a very deep valley exists along the [100] line. Second, a deep dip in the origin appears in both elemental and compound semiconductors. Third, the anisotropy is prominent and the dips are deep compared with conventional two-dimensional ACAR. Since these interesting shapes of the momentum distributions sensitively reflect the electronic

states in the materials, the analysis of the shapes provides important microscopic information on the electronic states in the materials.

The aim of this paper is to resolve the origin of these interesting features of the three-dimensional momentum distributions and to clarify what information can be extracted from analysis of experimental results of ACAR. We are especially interested in determining what information about vacancies can be provided by ACAR. For these purposes we perform first-principles calculations of the annihilation rates in the cases that the positron is in a perfect crystal of semiconductors and that the positron is captured by vacancies in Si. In the calculations of the annihilation rates, electron wave functions are obtained by using the norm-conserving pseudopotential method within the local-density approximation (LDA).[9] In obtaining the positron wave function, the potential energy for the positron is constructed from the valence-electron charge density unperturbed by the existence of the positron, from the core-electron charge density of the atomic LDA calculation, and from the point nuclear charges. Correlation interaction between electron and positron is neglected. Both electron and positron wave functions are expanded by a plane-wave basis set. We employ a supercell model to treat the case that the positrons are captured and are annihilated at vacancy sites.

For the case that the positrons are in a perfect crystal (Si and GaAs), important conclusions are (i) that our calculation for the momentum distribution successfully reproduces the observed valley along the [100] line and the dip around the origin and (ii) that the existence of both dip and valley can be qualitatively explained in terms of group theory.[10,11] For the case that the positron is captured by the vacancy, it is concluded that the valley and dip in the momentum distribution disappear. Since the momentum distribution in this case is very different from that in the case of perfect crystals, ACAR is a promising tool to detect vacancies in semiconductor crystals. Finally, we discuss the ratio of the lifetimes between the captured positron and the positron in the Bloch state.

The organization of this paper is as follows. We explain the calculational method in Sec. II. The calculated results are presented and discussed in Sec. III. We conclude the present work in Sec. IV.

II. METHOD

In this section we explain how the annihilation rates in semiconductors are calculated from the first principles. We first treat the case that a positron is in a perfect crystal. Within an independent particle approximation, the momentum distribution of the annihilation rates is given by

$$\rho(p)=\sum_n \left| \int_{\text{cell}} dr\, \Phi_p^n \Phi_+ \right|^2 , \tag{1}$$

where p is the momentum of the emitted photons, Φ_+ is the positron Bloch wave function, and Φ_p^n is the periodic part of the electron Bloch wave function at the p point in a Brillouin zone. It is noted that, if p is outside the first Brillouin zone (FBZ), the electron function can be obtained from that at a k point in FBZ by the relation

$$\Phi_p^n=\Phi_k^n \exp(iGr) , \tag{2}$$

where k in FBZ must satisfy the condition that $p-k=G$ for a certain reciprocal lattice vector G.

The evaluation of (1) is performed as follows. First, the valence-electron wave functions and the valence charge density are calculated from the self-consistent norm-conserving pseudopotential method within the LDA.[9] A Ceperley-Alder type of exchange-correlation potential is used,[12] and plane waves with kinetic energy up to 10 Ry are employed. The experimental lattice constants 5.42 and 5.65 Å for Si and GaAs, respectively, are used in the calculation. Second, the positron wave function is calculated, employing the same basis set as that of the electron wave functions. In this case the potential energy is constructed from the unperturbed valence electrons, from the frozen-core charge obtained within LDA, and from the nuclear point charge. The correlation between electron and positron is neglected. It is noted that the lowest positron state is at the Γ point. Third, using the obtained valence-electron and positron wave functions, we evaluate the annihilation rates in (1).

Next, we give a prescription to treat the case where a positron is captured by monovacancies in Si. In this case we employ the supercell model with the cell having the same shape as that of the diamond structure and containing 53 silicon atoms and one vacant site. As in the case of the perfect crystals, first the valence wave functions ϕ_n are calculated with a plane-wave basis set. In this case the cutoff energy is taken to be 5 Ry. The Γ point is taken as the sampling point of the Brillouin-zone integration. Second, the positron wave function ϕ_+ is obtained by calculating the lowest-energy level at the Γ point of the supercell model. Third, we evaluate the momentum distribution of the annihilation rates:

$$\rho(p)=\sum_n \left| \int_{\text{cell}} dr\, \phi_n \phi_+ \exp(ipr) \right|^2 , \tag{3}$$

where the summation is over occupied electron wave functions at the Γ point of the supercell. In evaluating the integration of (3), we place the vacant site in the center of the cell. In Sec. III we treat the case of the Jahn-Teller distorted vacancy (D_{2d}). In that case the principal axis of each vacancy created in the crystal is one of the three axes [001], [010], and [100]. In a real situation, the principal axes of the vacancies are statistically distributed among the three axes of the crystal. Thus we take a spatially averaged value for the annihilation rate.

In order to compare the lifetime of the captured positron with that of the positron in the perfect crystal, we evaluate the expression

$$\tau^{-1} \propto \int dp\, \rho(p)=\int dr\, \rho_e \rho_p , \tag{4}$$

where τ is the lifetime and ρ_e and ρ_p are the total charge densities of electrons and positrons, respectively. It is noted that the lifetime is short as the overlap integral in (4) becomes large.

III. RESULTS AND DISCUSSION

In this section we present the calculational results for the cases that positron is in Si and GaAs and that the positron is captured by vacancies in Si. The discussion based on group theory is also given for both cases. Finally, we discuss the lifetime and Doppler broadening spectrum of the captured positron.

A. Si and GaAs

Figure 1 shows the calculated square of the positron wave function in Si and GaAs. It is clear that the positron is located in the interstitial region and that the probability is low around the positions of the nuclei in both Si and GaAs. This is a consequence of the repulsive potential from the nuclear charges. The maximum point of the probability is found to be located at the tetrahedral site, which is the farthest from the nearest host atoms, and the values are 2.3 (2.4) positron per unit cell for Si (GaAs). Our finding that the maximum is at the tetrahedral site agrees with the result from the recent first-principles pseudopotential calculation for Si.[13]

In Figs. 2 and 3 the calculated electron-momentum distributions for Si and GaAs are shown. We have found the following three characteristics of the momentum distribution: First, a dip appears around the Γ point and a valley appears along the [100] line. Second, a maximum peak is located along the [110] line. Third, the annihilation rates are nearly equal to zero outside the Jones zone. These salient features are all consistent with the experimental distributions also shown in Figs. 2 and 3.

The origin of the above-mentioned dip and valley is now discussed from analysis based on group theory.[10,11] Since the positron is in the lowest-energy state, the wave function is totally symmetric; i.e., this function is invariant under any operation belonging to the symmetry group of the crystal. Therefore, we obtain an important rule that, unless the electron periodic function in (2) belongs to the totally symmetric representation of the space group at a given k, the annihilation rate is zero. Thus only functions whose representation is totally symmetric

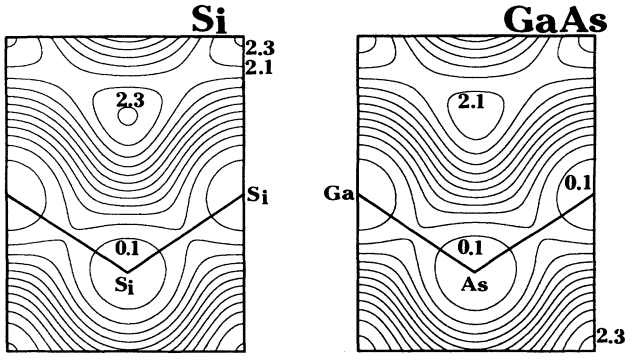

FIG. 1. Contour maps of the positron-charge densities in Si (left-hand side) and GaAs (right-hand side) on the $(1\bar{1}0)$ plane in units of particle per unit cell.

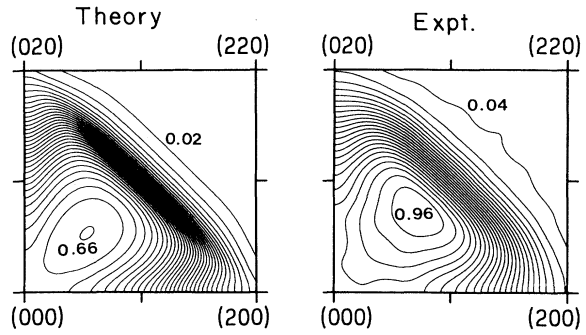

FIG. 2. Momentum distributions on the (001) plane for the perfect crystal of Si. The left-hand (right-hand) side is the theoretical [experimental (Ref. 8)] result. For the theoretical result, the values of the contour lines are equal to $\rho(p)$ in (1) and the spacing of the values is taken to be 0.02. For the experimental result, the values of the contour lines are normalized in order for the maximum value on the (001) plane to be 1, and the spacing of the values is taken to be 0.04. The position in the momentum space is represented in units of $2\pi/a$ with a being the lattice constant.

are annihilation active. In order to clarify which bands are annihilation active, we identify the representations of the wave functions in each valence band and tabulate the results in Table I, where the annihilation inactive bands are indicated by square brackets.

First, we study the case of Si (O_h^7), where 48 symmetry operations including glide and screw exist. Because this crystal is nonsymmorphic, special care is necessary in applying group theory: The annihilation active bands are different between the two areas depicted by A and B in Fig. 4. We give a brief comment on this point. It is known that the occurrence of sticking of bands at some zone edges is intrinsic to nonsymmorphic crystals.[14] In the present case, the sticking of totally and non-totally-symmetric bands occurs at the borderlines between areas A and B. It is emphasized that this sticking of the bands

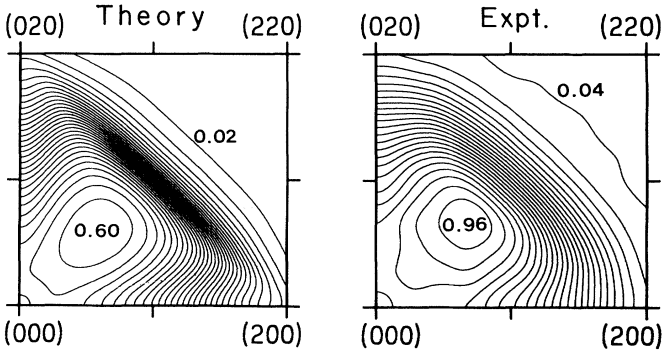

FIG. 3. Momentum distribution on the (001) plane for the perfect crystal of GaAs. The left-hand (right-hand) side is the theoretical [experimental (Ref. 8)] result. The units of the positions in the momentum space and of the contour lines are the same as in Fig. 2. The spacing of the values of the contour lines is also the same as in Fig. 2.

TABLE I. Representation of the periodic part of the valence Bloch wave in Si (O_h^7) and GaAs (T_d^2). The sequential number of the valence bands are given by the increasing order of the band energy. The square brackets indicate annihilation inactive bands and the parentheses annihilation active bands in GaAs which are revived by symmetry lowering from O_h to T_d. If the representations are different between areas A and B (see Fig. 4), the representation in area B is given in the lower space. It is noted that the third and fourth bands are degenerate on the Δ line in GaAs, though their representations are different from each other.

band			1	2	3	4
Si	Γ	O_h	a_1	$[t_{2g}]$	$[t_{2g}]$	$[t_{2g}]$
	Δ	C_{4v}	a_1	$[b_2]$	$[e]$	$[e]$
	∥[100]		$[b_2]$	a_1		
	Σ	C_{2v}	a_1	$[b_2]$	a_1	$[b_1]$
	∥[110]					
	(001) plane	C_s	a'	$[a'']$	a'	$[a'']$
			$[a'']$	a'	$[a'']$	a'
GaAs	Γ	T_d	a_1	$[t_2]$	$[t_2]$	$[t_2]$
	Δ	C_{2v}	a_1	(a_1)	$[b_1]$	$[b_2]$
			(a_1)	a_1		
	Σ	C_s	a'	(a')	a'	$[a'']$
	(001) plane	C_1	a	(a)	a	(a)
			(a)	a	(a)	a

is accompanied by the situation that the totally symmetric bands in area A (B) become non-totally-symmetric bands in area B (A). This situation is exemplified in Fig. 5: The first (third) and the second (fourth) bands cross at the point $(1,\frac{1}{2},0)$ in units of $2\pi/a$ (a is the lattice constant) and the crossover between the totally and the non-totally-symmetric representations occurs at the point on the borderline (the sequential numbers of the bands are given in increasing order of band energy).

At general points in areas A (B), except for the [100] line, the first (second) and third (fourth) bands are annihilation active. Therefore, two of the four valence bands are annihilation active at these points. On the other hand, only one band is annihilation active along the [100] line; that is, only the first (second) bands are annihilation active in area A (B) and the upper two bands are annihilation inactive on the whole line. This inactiveness of the upper two bands on the whole [100] line is due to the high symmetry of C_{4v} of this line and is the origin of the valley along the [100] line in the electron-momentum distribution in Fig. 2. Furthermore, the appearance of the dip at the Γ point in the momentum distribution is also attributed to these upper bands since they are inactive at the Γ point whose symmetry is also high (O_h). Figure 6, where the momentum distribution for the electrons in the upper two bands is presented, clearly shows that these

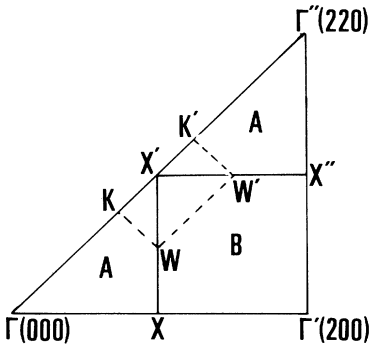

FIG. 4. (001) plane in the momentum space of Si. The X, W, and K points are at edges of the FBZ. The points indicated by the characters (except for Γ) with a single or double prime are at boundary points between higher zones. The borderlines between areas A and B consist of the $X-W$ line and of its corresponding lines between higher zones. The unit of the position is $2\pi/a$.

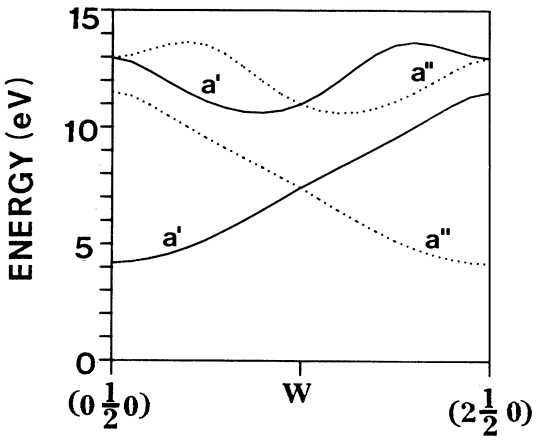

FIG. 5. Band structure of Si on the line from $(0,\frac{1}{2},0)$ to $(2,\frac{1}{2},0)$ in units of $2\pi/a$. The solid and dashed lines indicate annihilation-active and -inactive bands respectively. The absolute values of energies of the bands are taken as arbitrary.

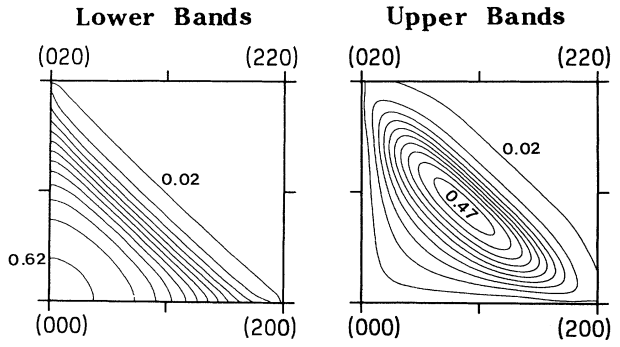

FIG. 6. Momentum distributions on the (001) plane for the annihilation with the electrons in the lower (left-hand side) and upper (right-hand side) two valence bands in Si. The units of the position in the momentum space are $2\pi/a$, and the values of the contour lines are equal to $\rho(p)$ in (1). The spacing of the values of the contour lines is taken to be 0.05.

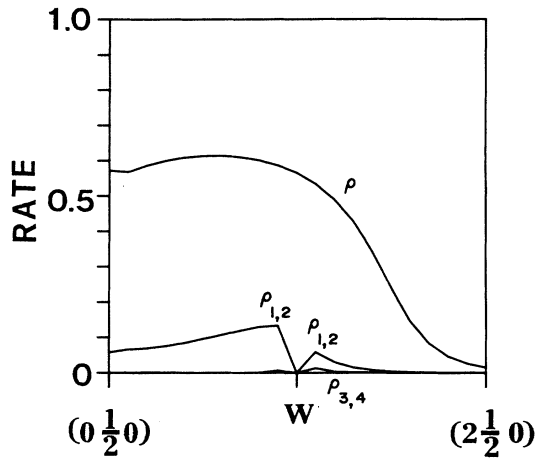

FIG. 7. Annihilation rates [$\rho(p)$] on the line from $(0,\frac{1}{2},0)$ to $(2,\frac{1}{2},0)$ in units of $2\pi/a$ in GaAs. $\rho_{1,2}$ and $\rho_{3,4}$ indicate the revived annihilation rates due to the lower and upper two bands, respectively (see explanation in the text).

two bands are the origins of the valley and dip. On the other hand, Fig. 6 also shows that the contribution of the lower two bands lets the valley and dip be shallow.

In the case of GaAs, the symmetry is lowered from O_h^7 to T_d^2: The two atoms in each unit cell are inequivalent to each other, and the number of symmetry operations is thus decreased from 48 to 24. Since the glide and screw operations are not included in this space group, this crystal is symmorphic. It is emphasized that symmetry lowering from O_h^7 to T_d^2 revives some of bands which are annihilation inactive in the case of Si (these revived bands are indicated by parentheses in Table I). If this symmetry-lowering effect is large enough, the ratio in the annihilation rate of the [110] line to the [100] one becomes small since one band additionally becomes annihilation active for both ridge [110] and valley [100] lines. However, it is found from the present calculation that the contribution of these revived bands to the annihilation rate is quite small, and thus prominent anisotropy also appears in the momentum distribution of GaAs. This situation is exemplified in Fig. 7: on the line $(0,\frac{1}{2},0)$–$(2,\frac{1}{2},0)$, the revived annihilation rates are almost negligible for the upper two bands ($\rho_{3,4}$ in the figure) and are small for the lower two bands ($\rho_{1,2}$). It is found that the annihilation rates from the upper two bands are very small at any point on the (001) plane. This relative insignificance of the symmetry-lowering effect (from O_h^7 to T_d^2) on the annihilation rate is a consequence from the fact that the valence orbitals of Ga are not very different from those of As.

Finally, we comment on the qualitative reliability of the present calculation. The calculated ratios of the annihilation rates between the maximum and Γ points are 1.03 and 1.13 for Si and GaAs. The corresponding experimental values are 1.19 and 1.18. This quantitative difference between theory and experiment is presumably due to the use of the electron pseudo-wave-functions in the present calculation. Although the pseudo-wave-function is accurate outside the core region, this function has no node and varies moderately within the core region, where the real wave function oscillates rapidly. Because of the difference within the core region between the real wave function and the pseudo-wave-function, the use of the pseudo-wave-function is not suitable when the exact evaluation of the integration in (1) is necessary. However, it is emphasized that, against the disadvantage of the use of the pseudo-wave-functions, the calculation performed with the present ingredients successfully reproduces the features of the experimental results. We owe this success to the fact that the positron wave function has low amplitude around the nuclei.

B. Si with neutral monovacancies

In this subsection we present the calculated results for the annihilation in Si with the neutral monovacancy. We first treat the case of the ideal vacancy of T_d symmetry. In Fig. 8 the calculated square of the positron wave function is shown. It is shown that the positron is localized around the vacancy site. This positron capture around the vacancy site is caused by the fact that the electron charge accommodated in the dangling bonds lowers the potential energy around the vacancy site, compared with that around the tetrahedral interstitial site in the perfect crystal. It is noted that the capture cannot be simply attributed to the difference between the vacancy and tetrahedral sites in the distance to the nearest Si atoms (the distance is identical for the two cases). Figure 9 shows the calculated momentum distribution for the annihilation of this captured positron. The distribution has a peak at the origin and is almost isotropic.

The shape of the above momentum distribution is now analyzed based on group theory. For this purpose we first determine the group consisting of the symmetry operations under which the function $\exp(ipr)$ in (3) is invariant. The determined group is the subgroup of the T_d point group (see Table II). Since both $\exp(ipr)$ and the positron wave function in (3) are totally symmetric in this

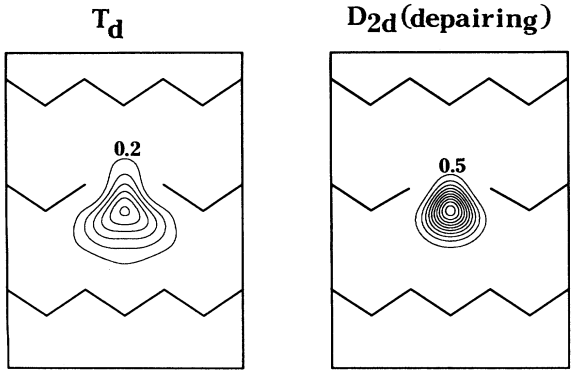

FIG. 8. Contour map, on the $(1\bar{1}0)$ plane in Si, of the square of the positron wave function captured by the ideal vacancy (left-hand side) and by the vacancy with depairing lattice distortions (right-hand side). The units of the contour values are particle per unit cell of Si. The spacing of the values of the contour lines is taken to be 0.2 (0.5) for the ideal vacancy (vacancy with the distortions). The maximum values of the contour lines are 1.2 and 5.0, respectively.

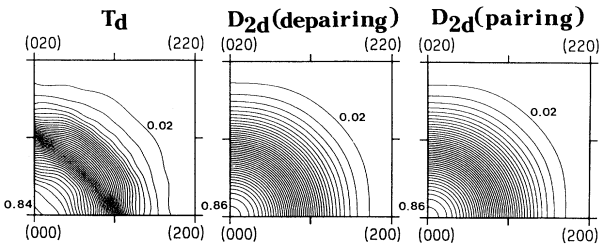

FIG. 9. Momentum distributions on the (001) plane for the case that the positron in Si is captured by the ideal vacancy (left-hand side) and by the vacancy with depairing (center) and pairing (right-hand side) lattice distortions. The units are the same as in Fig. 6. The spacing of the values of the contour lines is taken to be 0.02.

subgroup only electron wave functions which belong to the totally symmetric representation of the subgroup are annihilation active. Among the 106 occupied electronic levels at the Γ point in the present supercell model, the numbers of levels belonging to he A_1, A_2, E, T_1, and T_2 representations of the T_d point group are 10, 1, 16, 27, and 52, respectively. In Table II we show whether the wave functions belonging to the five representations are annihilation active or not at each p point of the (001) plane. In the case of representation E, the wave function is annihilation inactive on the [110] line and at the Γ point. As a result, the momentum distribution originating from the annihilation with the electrons having wave functions belonging to E show a very deep valley along the [110] line and a dip appears at the Γ point (see Fig. 10, where the momentum distribution for positron annihilation with electrons whose wave function belongs to each representation of the T_d group). The wave function belonging to T_1 is annihilation inactive at the Γ point and on the [100] line. Thus the momentum profile for these wave functions has a dip around the Γ point and a valley along the [100] line. The wave functions belonging to T_2 are inactive at the Γ point, so that the corresponding momentum distribution has a dip around the Γ point. The valley along the [100] line also appears in the T_2 case. This appearance of the valley is caused by the fact that only one (a_1) of the three wave functions (a_1, b_1, and b_2) is annihilation active on the line, while all three wave functions are annihilation active on the general points except for the high-symmetry points and lines as seen in Table II. As for the case of A_2, a dip and valleys along both [100] and [110] lines appear because the wave function is annihilation inactive for the point and lines. Since the wave functions of A_1 are annihilation active for all the points, the corresponding momentum distribution is isotropic and ha no dip at the Γ point. As is shown in Fig. 9, the momentum distribution of the annihilation rate for all the electrons has an almost isotropic shape and a dip around the Γ point. This is because the contribution from the A_1 wave functions is dominant. The slight anisotropy in the total-momentum distribution is due to the contribution from the wave functions of T_1 and T_2. Since the contribution from the wave functions of E is small, there is no valley along the [110] line in the total-momentum distribution. The contribution from the wave function of A_2 to the annihilation rate is very small [the maximum value of $\rho(p)$ for this wave function is found to be 0.01].

For the real neutral monovacancy, the Jahn-Teller effect[15] induces the symmetry-lowering distortion of the neighboring atoms around the ideal vacancy (T_d) because only two electrons occupy a triply degenerate gap level of the T_2 representation. In order to examine the effect of

TABLE II. Compatibility relation of representations of valence wave functions for the ideal vacancy (T_d). This table shows whether wave functions belonging to each representation of the T_d symmetry (i.e., A_1, A_2, E, T_1, and T_2) are annihilation active or not under the subgroup determined at a given line or point of the p space [Γ, Δ, Σ, and the (001) plane]. The square brackets indicate annihilation inactive.

Point	Subgroup	A_1	A_2	E	T_1	T_2
Γ	T_d	a_1	$[a_2]$	$[e]$	$[t_1]$	$[t_2]$
$\Delta\|\|[100]$	C_{2v}	a_1	$[a_2]$	$a_1+[a_2]$	$[a_2]+[b_1]+[b_2]$	$a_1+[b_1]+[b_2]$
$\Sigma\|\|[110]$	C_s	a'	$[a'']$	$2[a'']$	$a'+2[a'']$	$2a'+[a'']$
(001) plane	C_1	a	a	$2a$	$3a$	$3a$

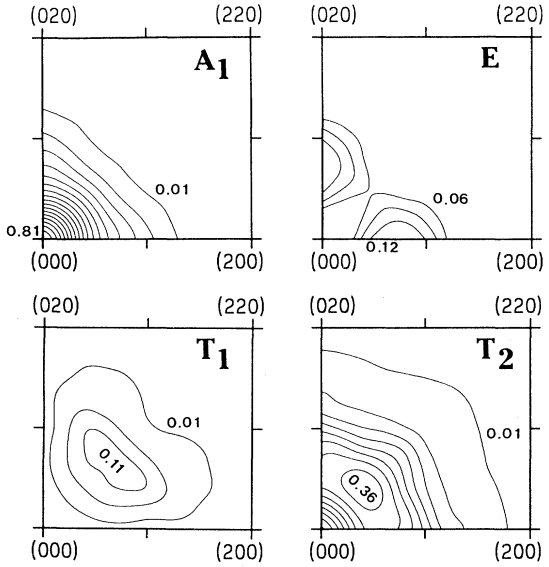

FIG. 10. Momentum distributions on the (001) plane of the positron annihilation in Si with vacancies. Each panel shows the contributions from the electrons whose wave function belongs to the A_1 (left and upper), E (right and upper), T_1 (left and lower), and T_2 (right and lower) representations in the T_d group. The units are the same as in Fig. 6. The spacings of the values of the contour lines are 0.05 for the A_1, T_1, and T_2 representations and 0.03 for the E representation.

this symmetry lowering on the momentum distribution, we perform calculations for the distorted vacancy in which the four nearest-neighbor Si atoms undergo the depairing Jahn-Teller distortion (0.11 Å) and inward-breathing displacements (0.28 Å). The amounts of these distortions were predicted from a first-principles calculation for the neutral monovacancy.[16,17] This depairing distortion, shown in Fig. 11, lowers the symmetry of the vacancy from T_d to D_{2d}.

The calculated square of the positron wave function for the Jahn-Teller distorted vacancy is shown in Fig. 8. The amplitude of the positron wave function is very localized by the inward distortion of the nearest Si atoms. Although the positron distribution of the distorted vacancy is very different from that of the ideal vacancy, the momentum distributions are similar to each other (see Fig. 9). We performed calculation for the pairing model (see Fig. 11) in which the amounts of the pairing and inward distortion of the nearest Si atom are the same as the corresponding values in the depairing model. It is found that the momentum distribution is also similar to that of the ideal vacancy as shown in Fig. 9. Therefore, it is concluded that the momentum distribution is not sensitive to lattice distortion around the vacancy. Moreover, the momentum distribution of the total annihilation rates of the positron captured by a vacancy is isotropic and has a peak at the origin. These features are drastically different from those in the case that the positron is annihilated in the perfect crystal. It is proposed from this difference that ACAR is an effective tool for the detection of vacancies in Si. Recently, an ACAR experiment[18] indeed shows that, when divacancies are created in Si by proton irradiation, the momentum distribution becomes isotropic and that the dip observed in the perfect crystal disappears.

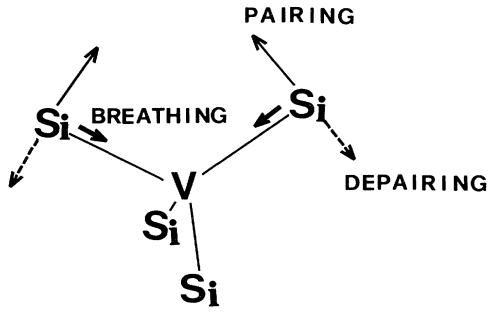

FIG. 11. Lattice distortion of the nearest Si atoms around the vacancy in Si. The three kinds of arrows indicate the symmetry-lowering pairing and depairing distortions and symmetry-conserving inward-breathing distortion.

C. Lifetime and one-dimensional momentum distribution in Si

Finally, we study the lifetimes and one-dimensional momentum distributions in the case that the positron is captured by the monovacancy. The calculational results of the lifetimes are tabulated in Table III, with experimental results and results obtained from the linear-muffin-tin-orbital Green's-function calculation[19] which was performed for the ideal vacancy.

The calculated ratios of the lifetime between the positron captured by the vacancy and the positron in the perfect crystal are 1.29 and 1.05 for the ideal and the depairing distorted vacancy, respectively (we also obtained the value of 1.05 for the pairing model). It is thus concluded that the lifetime of the captured positron is longer than that in the case of the perfect crystal, irrespective of the geometry of the vacancy. This conclusion is in agreement with experimental results that the lifetime of the captured positron (266–270 ps) is longer than that in the bulk (219 ps).[20,21] The reason for the longer lifetime of

TABLE III. Lifetime of the positron in Si. τ_{bulk} and τ_{vac} are the lifetimes of the positron in the perfect crystal and the positron captured by the monovacancy, respectively. $\lambda_{\text{core}}^{\text{vac}}$ is the ratio in the positron annihilation rate of the core electrons to the total electrons, in the case that the positron is captured by the vacancy. $\lambda_{\text{core}}^{\text{bulk}}$ is the corresponding value in the case of the perfect crystal.

	$\tau_{\text{vac}}/\tau_{\text{bulk}}$	$\lambda_{\text{core}}^{\text{vac}}/\lambda_{\text{core}}^{\text{bulk}}$	$\lambda_{\text{core}}^{\text{vac}}$	$\lambda_{\text{core}}^{\text{bulk}}$
Experiment[a]	1.21–1.23			
Theory (ideal vacancy)	1.29	0.82	0.047	0.057
Theory (depairing model)	1.05	0.30	0.017	
Theory (pairing model)	1.05	0.30	0.017	
Ref. 19 (ideal vacancy)	1.17	0.73	0.016	0.022

[a] References 20 and 21.

the captured positron is that the integral of the product of the electron and positron charges in (4) is small because of the low probability of electrons around the vacancy center at which the positron probability has the maximum value. In the case of the ideal vacancy, the maximum point of the overlap between the electron and positron charges is far from the vacancy center; the point is located at the bond-center site between the first- and second-nearest Si atoms. The distance between the vacancy site and maximum point is 2.96 Å. In the distorted vacancies, the calculated lifetimes become shorter because the inward motion of the nearest Si atoms enlarges the overlap integral in (4). The experimentally determined ratio of the lifetime of a captured positron to that in the perfect crystal is 1.21–1.23. This value is close to the calculated value (1.29) for the ideal vacancy and is larger than that (1.05) for the vacancy accompanied with the distortion. The amount of the distortion is determined from the first-principles calculation for the vacancy without the captured positron. It is thus plausible that upon positron capture the lattice relaxation around the vacancy is suppressed by the repulsive interaction between the captured positron and nuclei of the nearest Si atoms.

Finally, we discuss the shape of the one-dimensional momentum distribution in which the annihilation rate is integrated over the plane parallel to an axis. This distribution corresponds to the Doppler broadening spectrum obtained from the energy-resolved experiment. It is expected that, in this one-dimensional momentum distribution, a peak originating from annihilation with the valence electrons appears at the origin and that the peak is broadened from the minor contribution from the positron annihilation with the core electrons. Thus, first, we calculate the contribution from the core electrons to the total annihilation rate. The ratios in the annihilation rate of the core electrons and to the total electrons are found to be 0.057 for the perfect crystal and 0.047 (0.017) for the ideal vacancy (vacancy with the distortions). Thus the contribution from the core electrons to the annihilation rates is relatively small in the case that the positron is captured by the vacancy. These results indicate that, when vacancies are created in the crystal, the broadening effect from the annihilation of the core electrons is suppressed in the one-dimensional momentum distribution. Furthermore, the momentum distribution of the captured positron annihilated with the valence electrons is in a narrow momentum region compared with the positron in the perfect crystal (see Figs. 2 and 9). It is thus concluded that the peak in the one-dimensional momentum distribution is sharpened by the creation of vacancies. This sharpness is reflected on the value of so called S parameter (the ratio of the square measure near the peak to the whole area) in the Doppler broadening spectrum: The S parameter increases by the creation of vacancies.

IV. CONCLUSION

We have performed first-principles calculations of the momentum distribution of the positron-annihilation rates $\rho(p)$ in semiconductors. Our calculation successfully reproduces observed characteristic features of the momentum distributions in Si and GaAs. In Si, both of the upper two bands are annihilation inactive on the [100] line and at the Γ point because of high symmetries of the line (C_{4v}) and point (O_h), while one of the two bands are annihilation active at the other points on (001) plane. It is concluded that the appearance of valleys along the [100] line and of the dip around the Γ point is due to the annihilation inactiveness of the upper two bands. It is found that, in GaAs, the effect of symmetry lowering from O_h^7 to T_d^2 is very small and that the momentum distribution in GaAs thus resembles that of Si. In the case that the positron is captured by neutral monovacancies, the momentum distributions are found to be isotropic and to have a peak at the origin. Therefore, it is expected that ACAR is an effective tool for the detection of monovacancies. Moreover, it is suggested that ACAR is an effective tool as a sensitive microscopic probe of semiconductors. The lifetime of the captured positron is found to be sensitive to the breathing lattice distortion around the vacancy. It is suggested from the present theoretical result that the S parameter in the Doppler broadening spectrum increases when the vacancies are created in Si.

ACKNOWLEDGMENTS

We wish to acknowledge useful discussion with Dr. K. Kondo, Dr. J. -L. Lee, and Dr. Y. -K. Cho. One of the authors (M.S.) thanks Dr. T. Chiba for his valuable suggestion for the anisotropy of the momentum distributions in the case of the semiconductor perfect crystals. Two of the authors (M.S. and A.O.) also thank Dr. O. Sugino for a discussion on the Jahn-Teller effect on the neutral monovacancy.

[1]For example, see *Positron Annihilation,* edited by L. Dorikens-Vanpraet, M. Dorikens, and D. Segers (World Scientific, Singapore, 1989).
[2]D. Stround and H. Ehrenreich, Phys. Rev. **171**, 399 (1968).
[3]K. Fujiwara and T. Hyoudo, J. Phys. Soc. Jpn. **35**, 1133 (1973).
[4]M. A. Shulman, G. M. Beadsley, and S. Berko, Appl. Phys. **5**, 367 (1975).
[5]R. N. West, J. Mayers, and P. A. Walters, J. Phys. E **14**, 478 (1981).
[6]S. Tanigawa (unpublished).
[7]T. Chiba and T. Akahane, in *Positron Annihilation* (Ref. 1), p. 674.
[8]S. Tanigawa (unpublished).
[9]A. Oshiyama and M. Saito, J. Phys. Soc. Jpn. **56**, 2104 (1987); Phys. Rev. B **36**, 6156 (1987).
[10]P. E. Mijnarends, Physica **63**, 235 (1972).
[11]R. Harthoon and P. E. Mijnarends, J. Phys. F **8**, 1147 (1978).
[12]D. M. Ceperley and B. J. Adler, Phys. Rev. Lett. **45**, 566

(1980).
[13]C. Pennetta, Solid State Commun. **77**, 159 (1991).
[14]G. F. Koster, in *Space Groups and Their Representations,* Vol. 5 of *Solid State Physics* (Academic, New York, 1957), p. 173.
[15]G. A. Baraff, E. O. Kane, and M. Schlüter, Phys. Rev. B **21**, 5662 (1980).
[16]The depairing geometry is proposed in Ref. 17 from a first-principles supercell calculation with the cell containing 31 Si atoms. In this case the successive Jahn-Teller effect is active since the gap level belongs to the doubly degenerated E representation in the D_{2d} group. Since this Jahn-Teller distortion was found to be very small (<0.01 Å), the effect is neglected in the present calculation.
[17]O. Sugino (unpublished).
[18]S. Tanigawa (unpublished).
[19]M. J. Puska, O. Jepsen, O. Gunnarsson, and R. M. Nieminen, Phys. Rev. B **34**, 2695 (1986).
[20]S. Dannefaer, Phys. Status Solidi A **102**, 481 (1987).
[21]W. Fuhs, U. Holzhauser, S. Mantl, F. W. Richter, and R. Sturm, Phys. Status Solidi B **89**, 69 (1987).